ATINER CONFERENCE PAPER SERIES No: PHY-CHE-2013-0882

Athens Institute for Education and Research
ATINER

ATINER's Conference Paper Series
PHY-CHE-2013-0882

Deciphering the Kinetic and Gating Properties of Purinergic P2X7 Receptor Channels

Laurent Mackay
McGill University
Canada
Arthur Sherman
Lab Chief and Senior Investigator
Laboratory of Biological Modeling, National Institute of Diabetes and Digestive and Kidney Diseases, National Institutes of Health
USA
Stanko S. Stojilkovic
Lab Chief and Senior Investigator
Section on Cellular Signaling, National Institute of Child Health and Human Development, National Institutes of Health
USA
Anmar Khadra
Assistant Professor
McGill University
Canada

ATINER CONFERENCE PAPER SERIES No: PHY-CHE-2013-0882

Athens Institute for Education and Research
8 Valaoritou Street, Kolonaki, 10671 Athens, Greece
Tel: + 30 210 3634210 Fax: + 30 210 3634209
Email: info@atiner.gr URL: www.atiner.gr
URL Conference Papers Series: www.atiner.gr/papers.htm

ISSN **2241-2891**
23/1/2014

An Introduction to ATINER's Conference Paper Series

ATINER started to publish this conference papers series in 2012. It includes only the papers submitted for publication after they were presented at one of the conferences organized by our Institute every year. The papers published in the series have not been refereed and are published as they were submitted by the author. The series serves two purposes. First, we want to disseminate the information as fast as possible. Second, by doing so, the authors can receive comments useful to revise their papers before they are considered for publication in one of ATINER's books, following our standard procedures of a blind review.

Dr. Gregory T. Papanikos
President
Athens Institute for Education and Research

This paper should be cited as follows:

Mackay, L., Sherman, A., Stojilkovic, S.S. and Khadra, A. (2013) **"Deciphering the Kinetic and Gating Properties of Purinergic P2X7 Receptor Channels"** Athens: ATINER'S Conference Paper Series, No: **PHY-CHE-2013-0882.**

Deciphering the Kinetic and Gating Properties of Purinergic P2X7 Receptor Channels

Laurent Mackay
McGill University
Canada

Arthur Sherman
Lab Chief and Senior Investigator
Laboratory of Biological Modeling, National Institute of Diabetes and Digestive and Kidney Diseases, National Institutes of Health
USA

Stanko S. Stojilkovic
Lab Chief and Senior Investigator
Section on Cellular Signaling, National Institute of Child Health and Human Development, National Institutes of Health
USA

Anmar Khadra
Assistant Professor
McGill University
Canada

Abstract

possessing three intrasubunit orthosteric binding sites and unidentified number of allosteric binding sites. In previous work, we showed that the same receptor is capable of exhibiting sensitization and pore dilation (leading to the formation of biphasic currents and cell death) and/or desensitization (leading to a decline in current amplitude and cell life signaling) during sustained application of orthosteric agonists, depending on their concentrations. This was done in part by developing a 12-state Markov model consisting of naïve (not previously exposed to orthosteric agonist), desensitized, and sensitized/dilated states that reproduced whole-cell current recordings generated experimentally. In this model, we assumed that the occupancy of one or two ATP-binding sites of naïve receptors favored transition from open to desensitized states, whereas the occupancy of the third binding site favored receptor sensitization. Our goal here is to extend this modeling study by examining how these model cells behave under various ionic conditions in the medium, including those that contain large organic cation N-methyl-D-glucamine ($NMDG^+$) or divalent cation such as Ca^{2+}. We illustrate how the two main gating patterns behave under these ionic conditions and determine why the shift in reversal potential and the dilation of the channels are accompanied paradoxically by a decrease in the total conductance during voltage ramp protocols. The model adds more

evidence to our previous hypothesis, suggesting that dilation is masking desensitization. Our results also indicate that the allosteric sites through which divalent cations inhibit P2X7R should be extracellularly located.

Keywords: ATP-gated receptor-channels, orthosteric activation, pore dilation, receptor desensitization, allosteric inhibition.

Acknowledgment: This work was supported by the Intramural Research Program of the NICHD (Stojilkovic) and NIDDK (Sherman) of National Institute of Health, and Natural Sciences and Engineering Research Council of Canada (Khadra).

Introduction

Purinergic P2X receptors (P2XRs) are a family of ATP-gated non-selective cation channels, expressed in various cells, including neurons, myocytes and immune cells [4]. They play a crucial role in numerous physiological processes, including hormone secretion, muscle contraction and neurotransmission [11]. Abnormalities in them could lead to tissue inflammation and chronic pain [1]. In mammals, seven P2X subunits (termed P2X1-7) have been found and receptors are organized as trimeric homomers or heteromers [11], with three orthosteric agonist binding sites [10] that, when occupied by ATP, cause receptor activation and channel opening [9]. The kinetics of activation (rising phase of current), desensitization (decay of current in the presence of ATP) and deactivation (decay of current after removal of ATP) is receptor-specific [15].

The gating properties of P2X7Rs significantly differ from other receptors of this family. These receptors exhibit gradual and activation-dependent changes in their ion selectivity during sustained BzATP application [8], termed pore dilation. In dilated state, P2X7R pore is permeable to N-methyl-D-glucamine ($NMDG^+$), a large organic cation [12]. The receptor also exhibits increased sensitivity during repetitive agonist application, manifest as an increase in current amplitude with each agonist presentation separated by less than 30-min washout periods [14]. The activation phase of their current is either monophasic with slow growth when exposed to low BzATP doses ($< 32\,\mu M$), or biphasic with initially fast current growth followed by a slow growth when exposed to high BzATP doses ($\geq 32\,\mu M$) [12]. Furthermore, their dilation coincides temporally with the secondary slow growth of current, and is accompanied paradoxically by a decrease rather than an increase in the total conductance [12]. During sustained agonist application, their secondary current growth reaches a plateau with rate determined by agonist concentration (suggesting receptor sensitization) [12]. Finally, this receptor desensitizes during sustained application of orthosteric agonists, a process masked by pore dilation at high agonist concentrations and visible at low agonist concentrations [5].

These kinetic properties of P2X7R were captured and consolidated by developing initially an 8-state Markov model [14], that was later revised to a 12-state model [7], describing the binding and unbinding of BzATP molecules. The model explained the slow secondary growth of current during the activation phase, and the increase in current amplitude during repetitive simulation. The model also confirmed the hypothesis of P2X7R pore dilation, caused possibly by receptor phosphorylation, during stimulation with high agonist concentration, and illustrated the formation of memory (to previous agonist stimulation) responsible for receptor sensitization. Such mechanism may allow P2X7Rs to play a role in apoptosis (and inflammation) due to the absence of other mechanisms that can block the unrestricted and toxic Ca^{2+}-influx into the cells via these open or dilated channels. Furthermore, analysis of the P2X7R Markov model revealed that Ca^{2+}-independent desensitization is

masked by dilation [7] and that Ca^{2+} acts as an allosteric inhibitor for P2X7R by binding to unidentified allosteric binding site(s) [13].

Here we extend this study further to decipher the kinetics of these receptors under different ionic conditions and extend our study of Ca^{2+} allostery to determine if it is extracellular or intracellular. We use mathematical approaches that are based on biophysical data to answer such questions.

Mathematical Model

The details of the Markov model describing BzATP-agonist binding can be found in [14]. In brief, the model consists of 12 states (see Fig. 1), each representing the fraction of receptors that are either naïve (not previously exposed to BzATP), sensitized or desensitized with a given number of agonist binding sites occupied (identified by the black circles on each state in Fig. 1). Two of these states are naïve/closed (C_1, C_2), two are naïve/open (Q_1, Q_2) with conductance g_{12}, two are sensitized/closed (C_3, C_4), two are sensitized/open (Q_3, Q_4) with conductance g_{34} ($<g_{12}$) and four are desensitized/closed (D_1, D_2, D_3, D_4). Forward and backward rates between states within the same row are given by k_2, k_4, k_6 and k_1, k_3, k_5, respectively, whereas transition rates between naïve (middle row of Fig. 1) and sensitized (bottom row of Fig. 1) states and naïve and desensitized (top row of Fig. 1) states are L_1, L_2, L_3 and H_1, H_2, H_3, respectively. In this scheme, it is assumed that naïve states require at least two occupied binding sites for the channel to open. The differential equations associated with this Markov model are thus given by

$$\frac{dD_1}{dt} = k_1(2-F)D_2 - (3k_2AF + H_1)D_1 \quad (1)$$

$$\frac{dD_2}{dt} = 3k_2AFD_1 + 2k_3(2-F)D_3 + H_2C_2 - (k_1(2-F) + 2k_4AF + H_3)D_2 \quad (2)$$

$$\frac{dD_3}{dt} = 2k_4AFD_2 + 3k_5(2-F)D_4 + H_2Q_1 - (2k_3(2-F) + k_6AF)D_3 \quad (3)$$

$$\frac{dD_4}{dt} = k_6AFD_3 + H_2Q_2 - 3k_5(2-F)D_4 \quad (4)$$

$$\frac{dC_1}{dt} = H_1D_1 + k_1(2-F)C_2 + L_1C_4 - 3k_2AFC_1 \quad (5)$$

$$\frac{dC_2}{dt} = H_3D_2 + 3k_2AFC_1 + 2k_3(2-F)Q_1 - (k_1(2-F) + 2k_4AF + H_2)C_2 \quad (6)$$

$$\frac{dQ_1}{dt} = 2k_4AFC_2 + 3k_5(2-F)Q_2 - (2k_3(2-F) + k_6AF + H_2)Q_1 \quad (7)$$

$$\frac{dQ_2}{dt} = k_6AFQ_1 + L_2Q_3 - (3k_5(2-F) + L_3 + H_2)Q_2 \quad (8)$$

$$\frac{dC_4}{dt} = k_1(2-F)C_3 - (L_1 + 3k_2AF)C_4 \quad (9)$$

$$\frac{dC_3}{dt} = 3k_2AFC_4 + 2k_1(2 - F)Q_4 - (k_1(2 - F) + 2k_2AF)C_3 \quad (10)$$

$$\frac{dQ_4}{dt} = 2k_2AFC_3 + 3k_1(2 - F)Q_3 - (2k_1(2 - F) + k_2AF)Q_4 \quad (11)$$

$$\frac{dQ_3}{dt} = k_2AFQ_4 + L_3Q_2 - (3k_1(2 - F) + L_2)Q_3, \quad (12)$$

where A is the applied BzATP-agonist concentration (represented as a square wave) and

$$F = \alpha \frac{\beta^2}{\beta^2 + [DC]_e^2} \quad (13)$$

is a decreasing Hill function of extracellular divalent cation concentration $[DC]_e$, such as Ca^{2+} or Mg^{2+} (see Fig. 2 and [3]). It describes the 'allosteric' binding of extracellular DC to P2X7R, leading to a decrease in the forward (agonist-association) rates by a factor F and an increase in the backward (agonist dissociation) rates by a factor (2-F) when $[DC]_e$ is increased. The two parameters α and β in (13) represent the maximum level of 'allosteric' regulation (or inhibition) and the ½-maximum level of $[DC]_e$ required for such regulation, respectively.

The whole cell current in this case is given by

$$I = g_{12}(Q_1 + Q_2)(V - E_{12}) + g_{34}(Q_3 + Q_4)(V - E_{34}) \quad (14)$$

where V is the holding potential (–60 mV in all of the simulations here) and E_{12}, E_{34} are the reversal potentials of open (Q_1+Q_2) and dilated (Q_3+Q_4) states. The equation governing the concentration of intracellular Ca^{2+}, on the other hand, satisfies

$$\frac{d[Ca^{2+}]_i}{dt} = -f(\gamma SRI + k_c[Ca^{2+}]) \quad (15)$$

where f is the fraction of free calcium, γ converts the current to flux, S is calcium contribution to the current, R converts the current from A to pA, and k_c is the rate of calcium efflux. All parameter values and distributions are listed in Table 1.

The above model assumes that intracellular Ca^{2+} plays no role in P2X7R-allostery. We will show later that assuming otherwise will produce obvious inconsistencies with experimental recordings.

Receptor Activity in $NMDG^+$-only Containing Medium

It was shown in [12] that cells expressing P2X7Rs and bathed in $NMDG^+$-only containing medium respond to sustained agonist application (100 μM BzATP) initially with an outward current, lasting for few seconds, followed by an inward current until the end of the stimulation. This behavior was explained by suggesting that the outward current was generated by intracellular Na^+

leaving the cells through open P2X7R channels, while the inward current was induced by $NMDG^+$ entering the cell through dilated P2X7R channel pores. To verify this hypothesis, we assigned values for the reversal potentials E_{12} and E_{34} in the Markov model that were consistent with the reversal potentials of Na^+ and $NMDG^+$, respectively. As shown in Fig. 3A, applying the same stimulation protocol on the model successfully reproduced the outward current at the start of BzATP stimulation, because $E_{12}>V$, as well as the subsequent slow inward current, because $E_{12} < E_{34} < V$ when $NMDG^+$ is present, and $L_3=0.5\ s^{-1}$ is small.

We further examined this situation by applying voltage ramps from -80 mV to +80 mV twice per second for 25 s during 100 μM BzATP-agonist application (as shown in Fig. 3B) and plotted the I-V curves induced by this voltage-ramp protocol as was done experimentally. Figure 3C shows that the I-V curves gradually shifted from left to right (causing a decrease in the negativity of the reversal potential of these receptors) and their slopes paradoxically became shallower (i.e., decreased in value), indicating a decrease in ionic conductance. Such behavior is consistent with the experimental recordings in [12] and is similar to those observed in P2X2R recordings [2, [6], but no explanation was given as to why this was the case.

To explain the outcomes observed in Fig. 3A-C, we applied similar analysis to the one presented in [6], as follows. By rearranging the terms of Eqn. (14), we obtain

$$I = \left[g_{12}(Q_1+Q_2) + g_{34}(Q_3+Q_4)\right]\left[V - \frac{g_{12}(Q_1+Q_2)\,E_{12} + g_{34}(Q_3+Q_4)\,E_{34}}{g_{12}(Q_1+Q_2) + g_{34}(Q_3+Q_4)}\right] \quad (16)$$

or

$$I = g_{tot}(V - E_{tot}), \quad (17)$$

where the combined conductance is the sum of two conductances

$$g_{tot} = g_{12}(Q_1+Q_2) + g_{34}(Q_3+Q_4) \quad (18)$$

and the combined reversal potential is the weighted average of the two reversal potentials (with g_{tot} as the weight)

$$E_{tot} = \frac{g_{12}(Q_1+Q_2)E_{12} + g_{34}(Q_3+Q_4)E_{34}}{g_{12}(Q_1+Q_2) + g_{34}(Q_3+Q_4)} < 0. \quad (19)$$

Thus, to get the decline in the slopes of the I-V curves and the right-shift in reversal potential, g_{tot} and $|E_{tot}|$ (the absolute value of E_{tot}) must both decrease. We plotted the time evolution of these two quantities g_{tot} (black line) and $|E_{tot}|$ (gray line) in Fig. 4A, and found out that they were indeed strictly decreasing functions of time few milliseconds after the start of the 100-μM BzATP-agonist stimulation. This explained the observed shift in the reversal potential from that of Na^+ to $NMDG^+$, accompanied by a decrease in the combined conductance, despite pore dilation. Desensitization of P2X7R lay at the bottom of this phenomenon as some naïve and dilated receptors moved to the upper row of Fig. 1 during agonist stimulation and caused receptor channels to dilate but their combined conductance to decrease. Such outcomes confirmed our

previous hypothesis suggesting that dilation was masking desensitization in P2X7R, in contrast to P2X2 [6, 7]. It is important to point out here that this feature was very robust and did not depend on a delicate balance of parameters.

Current Simulations while Altering Ionic Conditions

Several whole-cell current recording experiments shown in [12] further support the hypothesis that P2X7R dilation occurs during extended BzATP-agonist stimulation with high ($\geq 32\,\mu M$) doses. These experiments were done by exchanging the ionic conditions in the medium, using an *Ultrafast Solution-Switching System*, to switch from Ca^{2+}-containing medium (Krebs-Ringer (KR)-like bath buffer [12]) to $NMDG^{+}$-only containing medium during BzATP-agonist stimulation. We applied similar protocols to the Markov model to examine if it can capture the observed effects of ionic exchanges and determine the underlying causes of these effects.

To achieve this goal, we multiplied the parameters that differ between Ca^{2+} and $NMDG^{+}$-only containing media in Table 1 by a Heaviside-step function, given by

$$H(t-t_i)=\begin{cases}0 & \text{if } t<t_i\\ 1 & \text{if } t\geq t_i\end{cases},\quad \text{where } i=1,2,3, \tag{20}$$

to capture the abrupt changes in the ionic concentrations in the medium at the time moments t_i, $i=1,2,3$. By simulating the application of 100 μM BzATP-agonist stimulation for 70 s and the replacement of the KR-buffer by $NMDG^{+}$ at $t_1=12$ s using Eqn. (18), we see in Fig. 3D that the fast exchange switched the inward current caused by Na^{+}, K^{+} and Ca^{2+} entry, to a Na^{+}-induced outward current due to the lack of $NMDG^{+}$-permeability at this point (since very few receptors were in the dilated states). We modified this protocol slightly by applying the ionic exchange twice: at $t_2=50$ s (when $NMDG^{+}$ was replaced by KR-buffer) and at $t_2=75$ (when the KR-buffer was restored) until agonist washout at $t=77$ s, and simulated the results in Fig. 3E. As shown, the presence of $NMDG^{+}$ in the medium significantly reduced the amplitude of the inward current due mainly to an increase in receptor desensitization (i.e., the shift to the upper row of Fig. 1). The removal of $NMDG^{+}$ from the medium, however, led to a fast recovery of the current amplitude before washout. All these results are identical to what has been observed in experimental recordings.

The advantage of the Markov model presented here is that we can track the time evolution of the various states in Fig. 1 and determine the underlying causes of these $NMDG^{+}$-induced effects. We did this by comparing the time evolution of the open (Q_1+Q_2) (solid) and dilated (Q_3+Q_4) (dashed) states under the two ionic exchange protocols discussed in Fig. 3D-E (black) to scenarios in which the medium remained consistently a KR-buffer (gray). As shown in Fig. 4B, the initial fast and slow rise in the open and dilated states,

respectively, produced by the first ionic exchange protocol, were identical to the one produced by the KR-buffer-only medium. However, when $NMDG^+$ was introduced into the medium in the former case, a significantly faster decline in the open states and a much lower rise in the fraction of dilated states were observed relative to the latter case. According to the model, this outcome results from the higher value of H_2 in the $NMDG^+$ case. The model thus suggests that the observed difference between the two cases was mainly due to the loss of a sizable fraction of receptors to the upper row of Fig. 1 (i.e., due to desensitization). Similar results were also observed in Fig. 4C in which the second exchange protocol was considered. Here the switch to $NMDG^+$ in the medium also increased the decline in the open and dilated states, with the former more significant than the latter, but not as significant as the previous exchange protocol, because many receptors were protected from desensitization by shifting to the bottom row of Fig. 1 (i.e., by dilating or sensitizing).

Allosteric Regulation of P2X7Rs by Divalent Cations

In this section, we focus on the dynamics of the Markov model in the presence of extracellular divalent cations (DCs) to examine their allosteric regulation of P2X7R gating. By allosteric regulation, we mean the binding of divalent cations to sites that are different from those that bind orthosteric agonists ATP and BzATP and casing modulation of receptor activity in the presence of orthosteric agonists. Recall that the decreasing Hill function F, given by Eqn. (13), was used to describe this allosteric inhibition by DCs.

We have previously demonstrated that the dose-response curve of current amplitude with respect to $[DC]_e$ was a decreasing Hill function [13], but we have never evaluated the downstream effect of this process on Ca^{2+} entry into the cell. We investigated this issue here by considering a heterogeneous population of model cells, each described by Eqns. (1)-(15) with parameters randomly selected from the distributions listed in Table 1, and evaluating the average of the maximum level of $[Ca^{2+}]_i$ attained by each model cell at different agonist concentrations. The dose-response curve of the average maximum level of $[Ca^{2+}]_i$ was then plotted with respect to agonist concentration when $[Ca^{2+}]_e$=2 mM (black) and when $[Ca^{2+}]_e$=0 mM (gray) (Fig. 5A). Both curves were fitted to increasing Hill functions of agonist concentration with $EC_{50} \approx 20$ and 12.6 μM, respectively. The leftward shift in the EC_{50} at low $[Ca^{2+}]_e$ was consistent with the results obtained in [3], in which Mg^{+2} was used as a DC.

The dependency of the expression F in Eqn. (13) on $[DC]_e$ implies that the allosteric DC-binding sites on the P2X7R were extracellular. This follows from the assumption that extracellular Ca^{2+} was playing the role of the allosteric regulator, rather than intracellular Ca^{2+}. Substituting $[DC]_e$ in Eqn. (13) with $[DC]_i$ (such as $[Ca^{2+}]_i$) would produce a biphasic dose response curve of the average maximum level of $[Ca^{2+}]_i$, not a Hill-like function (results not shown).

Such an outcome would be in disagreement with the experimental evidence presented in [3].

The efficiency of extracellular DCs in inhibiting P2X7Rs was then analyzed by quantifying the average maximum level of $[Ca^{2+}]_i$, evaluated over the same heterogeneous population of model cells used in Fig. 5A, as a function of $[DC]_e$. Applying 3 μM BzATP-agonist stimulation, resulted in a fitted curve to the simulated data that was a steadily decreasing Hill function with $EC_{50} \approx 6.5$ mM. These results confirm earlier suggestions that an increase in $[DC]_e$ caused an increase in allosteric inhibition of P2X7Rs [13].

Discussion

In this paper, we used mathematical modeling approaches to provide more support to two important aspects of P2X7R kinetics; namely, that desensitization is masked by dilation and that DC-allostery is likely to be extracellular than intracellular. We provided a mechanistic explanation, based on a 12-state Markov model, to explain how these receptors behave under various ionic conditions, including $NMDG^+$ and Ca^{2+}, and to examine the interaction between sensitization, desensitization and allostery.

The shift in the reversal potential observed during the application of the voltage ramp protocol and the generation of an outward current during BzATP application in $NMDG^+$-only containing medium followed by an inward current few seconds later were indicators of P2X7R-channel dilation. However, the decrease in the slopes of the I-V curves generated during the voltage ramp protocol indicated a decrease, rather than an increase, in the total conductance of these channels. We explained this by indicating that the discrepancy between the two experimental outcomes was mainly due to the desensitization of a small fraction of receptors, but this effect is concealed by receptors that are sensitizing. In other words, the increased conductance of the dilated states is negated by the lack of conductance of the desensitized states

The extracellular nature of DC-allostery was also very important feature that was essential for reproducing the experimental dose-response recordings that described the effects of Mg^{2+} and Ca^{2+} [13]. The model suggested that Ca^{2+} influx through open and dilated P2X7R channels, during BzATP-agonist stimulation, prevented intracellular Ca^{2+} from being an allosteric regulator. In fact, making F, described by Eqn. (13), depend on $[Ca^{2+}]_i$ would not only alter the dose response curves significantly (by making them biphasic), but also destroy the memory effect during repetitive stimulation that the model can successfully produce. In other words, the binding sites of DCs on these receptors appear to be extracellular. It remains to determine how many of these binding sites are actually available and how many must be occupied to inhibit the agonistic activity of BzATP.

References

[1] Abbadie, C., S. Bhangoo, Y. De Koninck, M. Malcangio, S. Melik-Parsadaniantz & F. A. White (2009). 'Chemokines and pain mechanisms.' *Brain Research Reviews* 60(1): 125-134.

[2] Chaumont S. & B. S. Khakh (2008). 'Patch-clamp coordinated spectroscopy shows P2X2 receptor permeability dynamics require cytosolic domain rearrangements but not Panx-1 channels.' *Proceedings of the National Academy of Sciences USA* 105(33): 12063-12068.

[3] Di Garbo, A., S. Alloisio & M. Nobile (2012). 'P2X7 receptor-mediated calcium dynamics in HEK293 cells: experimental characterization and modelling approach.' *Physical Biology* 9(2): 026001.

[4] Ding S. & F. Sachs (1999). 'Single channel properties of P2X2 purinoceptors.' *Journal of General Physiology* 113(5): 695-719.

[5] Egan, T. M., D. S. Samways & Z. Li (2006). 'Biophysics of P2X receptors.' *Pflügers Archiv - European Journal of Physiology* 452(5): 501-512.

[6] Khadra A., Z. Yan, C. Coddou, M. Tomić, A. Sherman & S. S. Stojilkovic (2012). 'Gating properties of the P2X2a and P2X2b receptor channels: experiments and mathematical modeling.' *Journal of General Physiology* 139(5): 333-348.

[7] Khadra, A., M. Tomić, Z. Yan, H. Zemkova, A. Sherman & S. S. Stojilkovic (2013). 'Dual gating mechanism and function of P2X7 receptor channels.' *Biophysical Journal* 104(12): 2612-2621.

[8] Khakh, B. S., X. R. Bao, C. Labarca & H. A. Lester (1999). 'Neuronal P2X transmitter-gated cation channels change their ion selectivity in seconds.' *Nature Neurosience* 2(4): 322-330.

[9] Koshimizu, T. A., F. Van Goor, M. Tomić, A. O. Wong, A. Tanoue, G. Tsujimoto & S. S. Stojilkovic (2009). 'Characterization of calcium signaling by purinergic receptor-channels expressed in excitable cells.' *Molecular Pharmacology* 58(5): 936-945.

[10] Nicke, A. (2008). 'Homotrimeric complexes are the dominant assembly state of native P2X7 subunits.' *Biochemical and Biophysical Research Communications* 377(3): 803-808.

[11] North, R. A. (2002). 'Molecular physiology of P2X receptors.' *Physiological Reviews* 82(4): 1013-1067.

[12] Yan, Z., S. Li, Z. Liang, M. Tomić & S. S. Stojilkovic (2008). 'The P2X7 receptor channel pore dilates under physiological ion conditions.' *Journal of General Physiology* 132(5): 563-573.

[13] Yan, Z., A. Khadra, A. Sherman & S. S. Stojilkovic (2011). 'Calcium-dependent block of P2X7 receptor channel function is allosteric.' *Journal of General Physiology* 138(4): 437-452.

[14] Yan, Z., A. Khadra, S. Li, M. Tomić, A. Sherman & S. S. Stojilkovic (2010). 'Experimental characterization and mathematical modeling of the P2X7 receptor channel gating.' *Journal of Neuroscience* 30(42): 14213-14224.

[15] Zemkova, H., M. L. He, T.A. Koshimizu & S. S. Stojilkovic (2004). 'Identification of ectodomain regions contributing to gating, deactivation, and resensitization of purinergic P2X receptors.' *Journal of Neuroscience* 24(31): 6968-6978.

Table 1. *Parameter values and distributions used in the simulations. Parameters with no values under $NMDG^+$ column are identical to those listed under the Ca^{2+} column (NA: not applicable). *Uniform distribution was used to account for the wide range of values attained by this parameter. #The mean is not the same as the default value to increase heterogeneity*

	Parameter Values and Distributions		
Symbol	**Values (Ca^{2+})**	**Values ($NMDG^+$)**	**Distribution**
$\mathbf{k_1}$	0.3 s^{-1}		Normal, σ=0.003
$\mathbf{k_2}$	40000 $(M.s)^{-1}$		Normal, σ=400
$\mathbf{k_3}$	2.4 s^{-1}		Normal, σ=0.024
$\mathbf{k_4}$	50000 $(M.s)^{-1}$		Normal, σ=500
$\mathbf{k_5}$	1.58 s^{-1}		Normal, σ=0.0158
$\mathbf{k_6}$	7000 $(M.s)^{-1}$		Normal, σ=70
$\mathbf{L_1}$	0.0001 s^{-1}		
$\mathbf{L_2}$	0.004 s^{-1}		Normal, σ=0.00004
$\mathbf{L_3}$	0.5 s^{-1}		Normal, σ=0.005
$\mathbf{H_1}$	0.001 s^{-1}		
$\mathbf{H_2}$	0.01 s^{-1}	0.25 s^{-1}	Normal, σ=0.0001
$\mathbf{H_3}$	0 s^{-1}		Normal, $\mu=0.001^{\#}$, σ=0.00001
α	1.67 (unitless)	NA	Normal, σ=0.0167
β	0.0024 M	NA	Normal, $\mu=0.005^{\#}$, σ=0.00005
f	0.05 (unitless)	NA	Uniform, $[0.01,0.05]^*$
γ	$5x10^{-6}$ μM/(s · pA)	NA	
S	10^{-3} (unitless)	NA	
R	10^{12} (unitless)	NA	
$\mathbf{k_c}$	4 s^{-1}	NA	
$\mathbf{g_{12}}$	$1.5x10^{-8}$ S		Normal, $\sigma=1.5x10^{-10}$
$\mathbf{g_{34}}$	$4.5x10^{-8}$ S		Normal, $\sigma=4.5x10^{-10}$
V	-0.06 V		
$\mathbf{E_{12}}$	0 V	-0.067 V	
$\mathbf{E_{34}}$	0 V	-0.045 V	

.

Figure 1. *The 12-state Markov model describing the binding and unbinding of BzATP-agonist to P2X7R. The top row represents the desensitized states, middle row represents the naïve states and bottom row represents the sensitized states. The states C_i and D_i are closed (i=1, 2, 3, 4), whereas Q_1, Q_2 are open and Q_3, Q_4 are dilated. White (black) circles are the unoccupied (occupied) agonist binding sites*

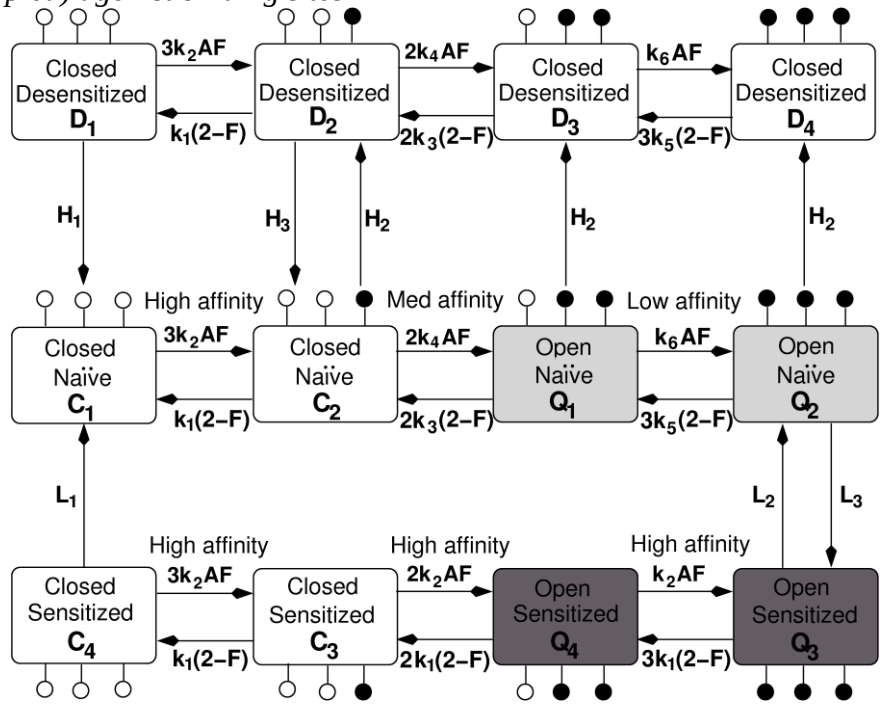

Figure 2. *The graph of the two Hill functions F and (2-F) describing the allosteric effect of divalent cations on P2X7R*

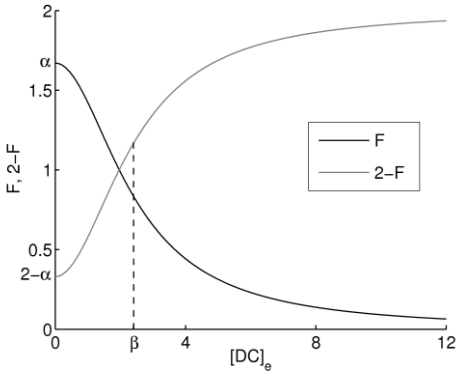

Figure 3. *Current simulations generated by 100 μM BzATP application in the presence of $NMDG^+$ in the medium under the following conditions: (A) 40-s BzATP stimulation in $NMDG^+$-only containing medium; (B) 25-s BzATP stimulation in $NMDG^+$-only containing medium and under the ramp protocol; (C) I-V curves obtained from the ramp protocol applied in B; (D) 70-s BzATP stimulation and the exchange of the KR-buffer medium with $NMDG^+$-only containing medium at $t_1 = 12$ s; (E) 67-s BzATP stimulation and the exchange of extracellular ionic conditions in the medium from KR-buffer to $NMDG^+$ at $t_2 = 50$ s, then back to KR-buffer at $t_3 = 75$ s*

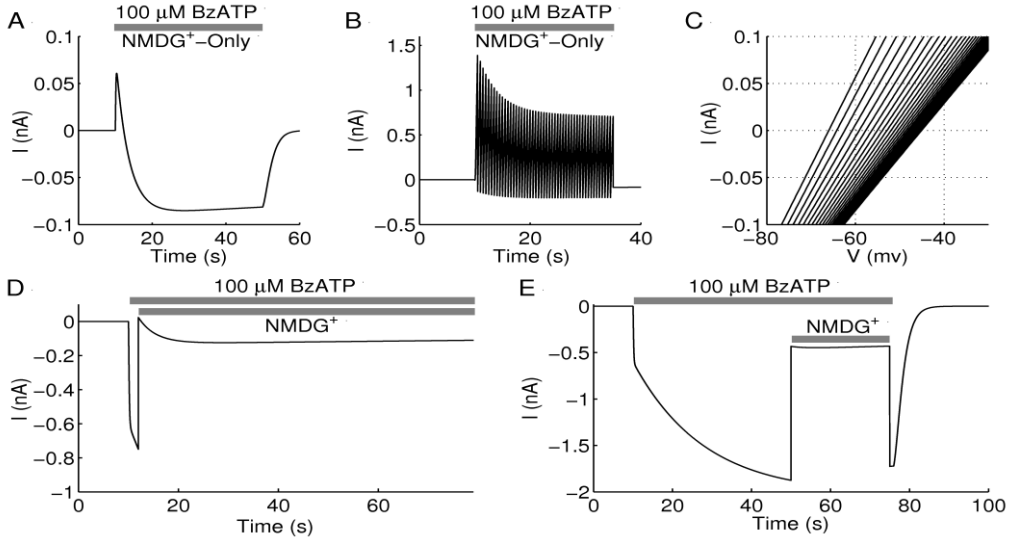

Figure 4. *(A) The time evolution of the combined conductance g_{tot} (black/left-ordinate) and combined reversal potential E_{tot} (gray/right-ordinate). (B-C) The time evolution of the open (Q_1+Q_2) (solid/black) and dilated (Q_3+Q_4) (dashed/black) states associated with the current simulations presented in Fig. 3D (B), and Fig. 3E (C). The gray bars show the duration of BzATP application or the duration in which $NMDG^+$ is present in the medium. The gray curves in panels B and C show the time evolution of the open (solid) and dilated (dashed) states in the absence of alterations in extracellular ionic conditions, i.e., in the presence of KR-buffer and absence of $NMDG^+$ in the medium.*

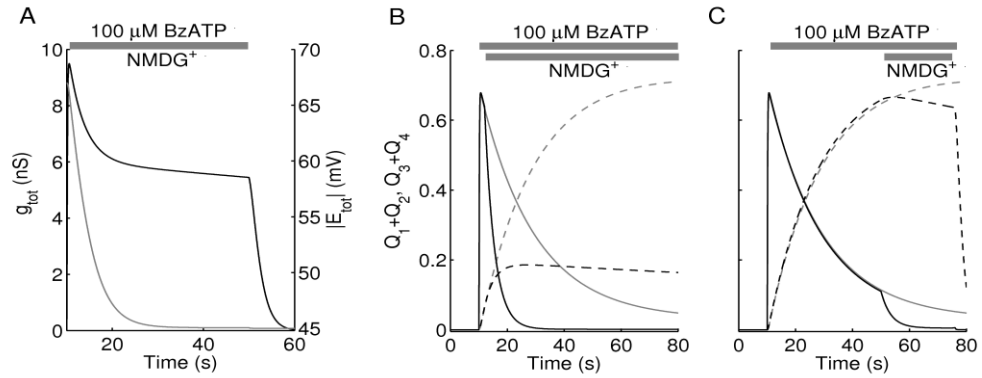

Figure 5. *The dose response curves of (A) the maximum $[Ca^{2+}]_I$ as a function of BzATP concentration during 40-s stimulation and under the following ionic conditions in the medium: $[DC]_e$=2 mM (black) and $[DC]_e$= 0 mM (gray); and (B) the maximum $[Ca^{2+}]_i$ as a function of $[DC]_e$ during 3 μM 40-s BzATP-agonist stimulation. Here $[DC]_e$ =$[Ca^{2+}]_e$. These dose response curves were generated from a heterogeneous population of cells obtained by randomly selecting parameters from the distributions listed in Table 1. Error bars represent ±SEM.*